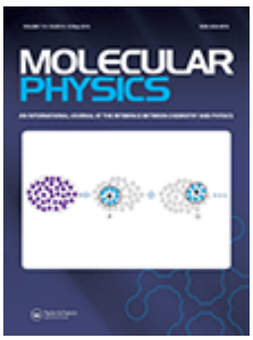

Taylor & Francis
Taylor & Francis Group

Molecular Physics

An International Journal at the Interface Between Chemistry and Physics

ISSN: 0026-8976 (Print) 1362-3028 (Online) Journal homepage: https://www.tandfonline.com/loi/tmph20

High-resolution spectroscopy of the $A^+\,^2\Pi \leftarrow X^+\,^2\Sigma^+$ transition of MgAr+ by isolated-core multiphoton Rydberg dissociation

M. Génévriez, D. Wehrli & F. Merkt

To cite this article: M. Génévriez, D. Wehrli & F. Merkt (2019): High-resolution spectroscopy of the $A^+\,^2\Pi \leftarrow X^+\,^2\Sigma^+$ transition of MgAr+ by isolated-core multiphoton Rydberg dissociation, Molecular Physics, DOI: 10.1080/00268976.2019.1703051

To link to this article: https://doi.org/10.1080/00268976.2019.1703051

MOLECULAR PHYSICS e1703051
https://doi.org/10.1080/00268976.2019.1703051

Taylor & Francis
Taylor & Francis Group

RESEARCH ARTICLE

High-resolution spectroscopy of the $A^+\,^2\Pi \leftarrow X^+\,^2\Sigma^+$ transition of $MgAr^+$ by isolated-core multiphoton Rydberg dissociation

M. Génévriez, D. Wehrli and F. Merkt

Laboratory of Physical Chemistry, ETH Zurich, Zurich, Switzerland

ABSTRACT

We report on a new measurement of the $A^+\,^2\Pi_{\Omega'=1/2,3/2} \leftarrow X^+\,^2\Sigma^+$ electronic transition of $MgAr^+$. The experiment relied on the resonance-enhanced multiphoton dissociation of the isolated ionic core of Rydberg MgAr molecules. The dissociation mechanism leading to the production of Mg atoms in high Rydberg states was used to separate the dissociation signal from the background and record background-free spectra. The rotational structure of the measured vibrational bands was partially resolved, and values of the rotational constants and band origins were extracted from the spectra.

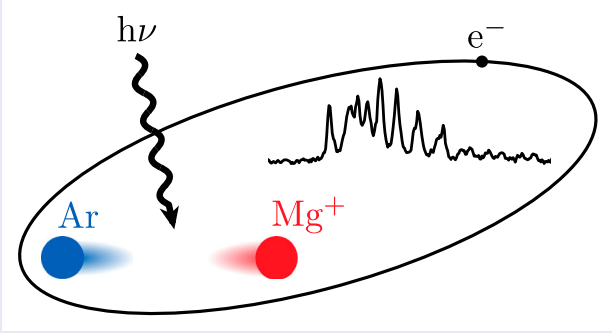

ARTICLE HISTORY
Received 4 November 2019
Accepted 1 December 2019

KEYWORDS
Rydberg molecule; ion spectroscopy; multiphoton dissociation; $MgAr^+$

1. Introduction

The $MgAr^+$ molecular ion has been studied in a series of experiments by Duncan and coworkers [1–4] with the aim of spectroscopically characterising this system and investigating elementary processes in metal-ligand interactions and metal-ion solvation [5]. These works stimulated theoretical calculations which, in most cases, fell in good agreement with experimental data and provided insights into the structure of the ground and first electronically-excited states of the $MgAr^+$ ion [6–10]. These efforts led to the understanding that, in $MgAr^+$ and more generally in small metal-rare-gas ionic complexes, the charge is localised on the metal atom and bonding is predominantly the result of electrostatic interactions [2,5,7], which are of charge-induced-dipole nature in $MgAr^+$.

We recently carried out a spectroscopic study of the ground electronic state of $MgAr^+$ ($X^+\,^2\Sigma^+$) by pulsed-field-ionisation zero-kinetic-energy photoelectron spectroscopy (PFI-ZEKE-PES) [11]. Vibrational levels from $v'' = 2$ to $v'' = 9$ were observed for the first time, which enabled the derivation of the potential-energy function of the X^+ state. In the present article, we extend our work to the first electronically excited state of $MgAr^+$ ($A^+\,^2\Pi$) and report data that complement those reported in Refs. [1–4].

Extending our PFI-ZEKE-PES study of the X^+ state to the A^+ state would require the use of vacuum-ultraviolet (VUV) radiation. However, table-top VUV sources possess low fluences which are incompatible with the low density of MgAr molecules ($<10^8$ cm^{-3}) produced in our experiment. Another experimental scheme was therefore adopted, which relies on the resonance-enhanced multiphoton dissociation (REMPD) of the ionic core of Rydberg MgAr molecules. REMPD [12,13] is a technique widely used to study excited states of molecular ions (see

CONTACT M. Génévriez matthieu.genevriez@phys.chem.ethz.ch Laboratory of Physical Chemistry, ETH Zurich, CH-8093 Zurich, Switzerland

[5,14,15] and references therein). In molecular Rydberg states of sufficiently high principal quantum number ($n \geq 80$ in the present work), the ionic core behaves independently of the Rydberg electron, i.e. it can be considered *isolated*. In this case, we expect the REMPD of the ionic core to closely resemble that of the bare ion, with the difference that the Rydberg electron may remain weakly attached to the charged fragment after core dissociation [16,17]. In this case, one may use the term isolated-core multiphoton Rydberg dissociation in analogy to the method of isolated-core-excitation spectroscopy used to study autoionizing Rydberg states of alkaline-earth metal atoms [18–21]. This property can be exploited to discriminate dissociation products from background ions (here Mg^+), resulting in a background-free measurement. This advantage was exploited, for example, by Krause and Neusser, to determine the dissociation energies of benzene-rare-gas dimers in mass-analysed-threshold-ionisation (MATI) experiments [22,23].

The present paper reports a study of the $A^+\ ^2\Pi_{\Omega'=1/2,3/2}(v'=0,1,5) \leftarrow X^+\ ^2\Sigma^+(v''=3)$ transitions of $^{24}MgAr^+$ and the $A^+\ ^2\Pi_{\Omega'=1/2}(v'=1) \leftarrow X^+\ ^2\Sigma^+(v''=3)$ transition of $^{25}MgAr^+$ by isolated-core multiphoton Rydberg dissociation spectroscopy. The experimental setup is briefly described in Section 2. The experimental scheme for isolated-core multiphoton Rydberg dissociation is discussed in detail in Section 3. The measured spectra are presented in Section 4, along with the analysis of the rotational structure of the vibrational bands. Rotational constants of the initial and final states, together with band origins, are reported and compared to earlier data. The spectator nature of the Rydberg electron in the core-excitation and dissociation processes is verified experimentally.

2. Experimental setup

The experimental setup has been described in detail previously [11]. Briefly, MgAr molecules are formed by laser ablation of a Mg rod with the second harmonic of a pulsed Nd:YAG laser within the nozzle of a pulsed-supersonic-expansion source, with Ar used as the carrier gas. The supersonic-expansion conditions allow these molecules to be rotationally cooled and transported toward the photoexcitation region. The molecular beam is collimated, 8 cm downstream from the nozzle, by a 3-mm-diameter skimmer before it enters the photoexcitation chamber. The MgAr molecules formed in the source are almost exclusively in the metastable $Mg(3s3p)\cdot Ar\ a\ ^3\Pi_0(v=0)$ state and their rotational temperature is estimated to be 3 K [11].

In the photoexcitation chamber, the molecular beam is intersected at right angles by the pulses from two Nd:YAG-pumped dye lasers. The first laser, hereafter called laser 1, is operated with the dye Styril 8 and its fundamental output is frequency tripled using two β-barium-borate (BBO) nonlinear crystals. The wave number $\tilde{\nu}_1$ of the frequency-tripled radiation can be continuously tuned in the range from 38,700 cm^{-1} to 39,500 cm^{-1}, its bandwidth is 0.15 cm^{-1} and the pulse energy is 0.2 mJ. The second laser, hereafter called laser 2, is operated with the dye DCM and its fundamental output is frequency-doubled with a BBO crystal. The frequency-doubled output has a bandwidth lying below 0.1 cm^{-1}, its pulse energy is attenuated to below 50 μJ to reduce power broadening, and its wave number $\tilde{\nu}_2$ can be continuously tuned in the range from 31,100 cm^{-1} to 32,600 cm^{-1}. Both lasers are linearly polarised along a direction perpendicular to the direction of propagation of the molecular beam. The wave numbers of the fundamental outputs of both dye lasers are measured with a commercial wave metre with a specified absolute accuracy of 0.02 cm^{-1}.

The photoexcitation of MgAr molecules occurs inside a 5.8-cm-long stack of five equally-spaced and resistively-coupled cylindrical electrodes. The stack is surrounded by two concentric mu-metal shields to suppress stray magnetic fields. After interaction with the lasers, a small electric-field pulse of 1.7 V/cm is applied to the stack for 6 μs, followed by a large extraction pulse of 130 V/cm. The extraction pulse accelerates all positively charged particles into a linear time-of-flight (TOF) region, at the end of which they are detected by a micro-channel-plate (MCP) detector. The MCP signal is amplified and recorded on a fast digital oscilloscope, itself connected to a computer for data processing and analysis. The experiment is operated at a repetition rate of 25 Hz.

3. Isolated-core multiphoton Rydberg dissociation

Previous experimental studies of the $A^+\ ^2\Pi_{\Omega'=1/2,3/2} \leftarrow X^+\ ^2\Sigma^+$ transitions of $MgAr^+$ were carried out by laser photodissociation spectroscopy of $MgAr^+$ molecules in the $v''=0$ and 1 vibrational levels of the $X^+\ ^2\Sigma^+$ state [1–4]. The dissociation of the molecular ions was attributed to a (1+1) resonance-enhanced multiphoton dissociation (REMPD) process in which ground-state ions were first excited to the A^+ state and then dissociated into Mg^+ and Ar by absorption of a second photon. The experiments were carried out using a mass-selected beam of ground-state $MgAr^+$ ions. By monitoring the Mg^+ yield as a function of the frequency of the excitation laser, vibrationally and rotationally resolved spectra could be recorded [4]. In the present experiment, a neutral beam

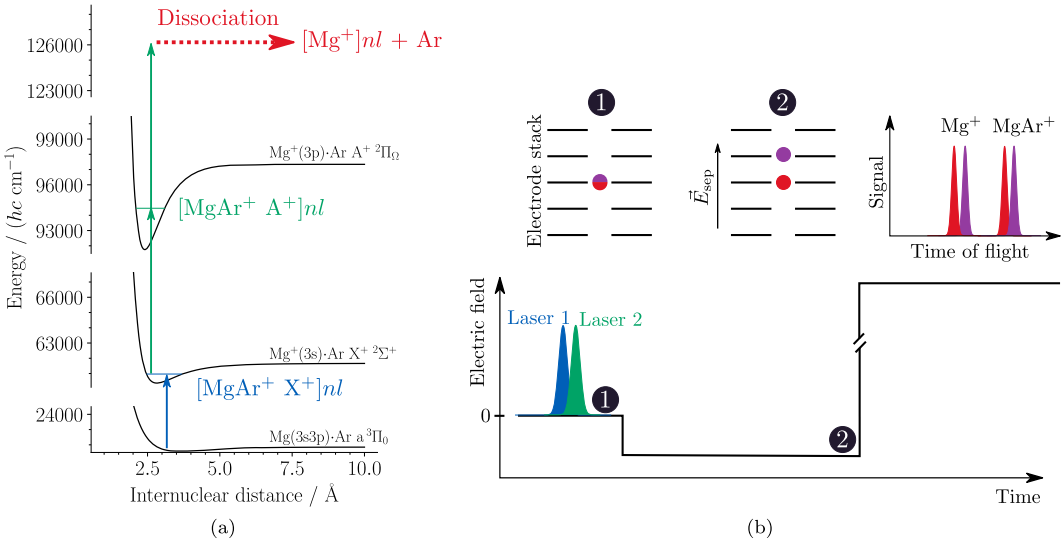

Figure 1. (a) Schematic diagram of the energy-level structure and excitation scheme used to record the isolated-core multiphoton Rydberg dissociation spectrum of the $A^+ - X^+$ transition of $MgAr^+$. The potential energy functions of the relevant electronic states of the neutral molecule and the ion are depicted by the solid black curves. The notation $[MgAr^+\ X^+, A^+]nl$ denotes a Rydberg state of the neutral molecule in which the ion core is in the X^+ (A^+) electronic state. The energy scale is relative to the energy of $Mg(3s^2\ ^1S_0)$. (b) Electric-field pulse sequence used in the experiment. The positions of the Rydberg particles (red) and ions (purple) within the electrode stack at different times are indicated on the upper part of the figure. A schematic view of the signal at the MCP detector is shown on the upper right.

is used instead of an ion beam. Other species present in the beam, including Mg atoms and $MgAr_n$ clusters, can be nonresonantly ionised and dissociated by lasers 1 and 2. The large number of resulting Mg^+ background ions obscures the small Mg^+ signal originating from REMPD events. Therefore, the earlier REMPD scheme [1–4] cannot be used in the present experiment. Instead, we follow another approach in which $[MgAr^+\ X^+]nl$ Rydberg states are first produced by photoexcitation of neutral MgAr molecules in their a $^3\Pi_0$ metastable state. The ion core is subsequently fragmented in a resonance-enhanced multiphoton dissociation process taking place within the Rydberg-electron orbit. For a sufficiently high principal quantum number n of the Rydberg electron, the ionic core of the Rydberg molecule can be regarded as isolated and the excitation of the ionic core from the X^+ to the A^+ state is expected to be equivalent to that of the bare ion.

The excitation and dissociation scheme is depicted in the left panel of Figure 1. In a first step, MgAr molecules in the metastable a $^3\Pi_0$ state are excited to Rydberg states belonging to series converging to a selected $X^+\ ^2\Sigma^+(v'')$ state of the ion ($v'' = 3$ for the data presented below). The excitation is carried out with the light pulse from laser 1, the wave number of which is set just below the $v'' = 3$ ionisation threshold (39,027.1 cm^{-1} [11]). In a second step, after ~10 ns, the light pulse from laser 2 excites the ionic core of the Rydberg molecule from the $X^+\ ^2\Sigma^+(v'')$ state to a dissociative state in a (1+1) resonant two-photon excitation process *via* the $A^+\ ^2\Pi_{\Omega'}(v')$ intermediate state. The time separation between the pulses from laser 1 and 2 ensures that excitation occurs in a sequential manner. There are three possible decay mechanisms for the core-excited Rydberg molecule in the dissociative state: (i) autoionisation: the Rydberg electron is ejected and the ion core relaxes to a lower-lying, non dissociative state; (ii) dissociative autoionisation: the Rydberg electron is ejected and the molecular ion dissociates; (iii) dissociation: the neutral Rydberg molecule dissociates into a ground state Ar atom and a Mg atom in a Rydberg state ($[Mg^+]nl$). We include in mechanism (ii) the situation in which, after dissociation of the molecule into two neutral fragments, the Mg atom is left in a core-excited Rydberg state which rapidly autoionizes. If, instead, the Mg core-excited Rydberg state decays by fluorescence of the core to the ionic ground state, the decay mechanism leads to the formation of long-lived Rydberg states of Mg and is considered to contribute to mechanism (iii). The branching ratios between these mechanisms are governed by the relative magnitude of the autoionisation, dissociation and fluorescence rates of the states under consideration. Core-excited Rydberg molecules with the ion core in the A^+ state can also decay by autoionisation and predissociation. However, for the high n values used in our experiments, these processes are negligible (see Section 4).

Mechanism (iii) results in the production of neutral $[Mg^+]nl$ Rydberg atoms, whereas all other decay mechanisms produce Mg^+ or $MgAr^+$ ions. This difference can be exploited to detect the excitation from the X^+ state to the A^+ state in a background-free manner by monitoring the delayed pulsed-field ionisation (PFI) of the $[Mg^+]nl$ fragments. By applying a weak electric field of 1.7 V/cm across the electrode stack after the interaction with the laser pulses, all prompt Mg^+ and $MgAr^+$ ions are swept out of the interaction region, regardless of how they were produced, whereas $[Mg^+]nl$ Rydberg atoms remain unaffected by the field (see right panel in Figure 1). Indeed, a field strength of 1.7 V/cm is not large enough to field ionise Rydberg states with $n < 120$. After 6 µs, the large extraction electric-field pulse applied to the stack (130 V/cm) field ionises all Rydberg atoms and molecules and accelerates the resulting ions onto the detector. The spatial separation between the ions generated by PFI and background ions makes it possible to distinguish them by their times of flight. By recording the Mg^+ ions produced by delayed PFI as a function of the wave number of laser 2, the resonance-enhanced photodissociation of the $MgAr^+$ core *via* the A^+ intermediate state can be recorded in a background-free manner.

The present photoexcitation and photodissociation scheme is closely related to the technique of fragment-photoinduced-Rydberg-ionisation (fragment-PIRI) spectroscopy [24]. In both cases, neutral molecules are first prepared in a Rydberg state and their ionic core is later photodissociated. In fragment-PIRI spectroscopy, however, photodissociation occurs after the separation of the prompt ions by the small discrimination electric-field pulse. This detection scheme has the advantage that it is applicable to molecules for which mechanism (iii) is weak or even nonexistent. However, it does not allow background ions with the same mass as the fragment (here Mg^+) produced by the dissociation laser to be separated from the dissociation signal. The present method uses an electric-field pulse sequence identical to the one used in MATI spectroscopy [25]. Previous works dedicated to the study of Rydberg dissociation with MATI dealt only with the ion core in its ground electronic state [22,23]. Photoexcitation was therefore carried out to the dissociative Rydberg state directly, by single- or multi-photon absorption. In the present case, we study the electronic excitation of the ion core *after* the molecule has been excited to a Rydberg state, and therefore use two appropriately delayed laser pulses to excite the Rydberg electron and the ion core sequentially. The excitation of the neutral molecule to a Rydberg state prior to the photodissociation of the isolated core offers the additional advantage that the ion core can be prepared in a selected vibrational state. We exploited this advantage by recording spectra of the $A^+ - X^+$ transitions from a selected level ($v'' = 3$) of the X^+ state.

4. Results and discussion

We have recorded the spectra of transitions from the $X^+\,^2\Sigma^+(v'' = 3)$ state to the $A^+\,^2\Pi_{\Omega'=1/2,3/2}(v')$ states of $^{24}MgAr^+$ with $v' = 0, 1$ and 5. An example of such a spectrum is shown in Figure 2 and corresponds to $v' = 1$ and $\Omega' = 3/2$. It depicts the yield of $^{24}Mg^+$ ions produced by delayed pulsed-field ionisation as a function of the wave number of the core-excitation laser (laser 2). The spectrum was recorded after excitation of the neutral molecule to $[MgAr^+\ X^+(v'' = 3)]nl$ Rydberg states with the wave number of laser 1 set to $\tilde{\nu}_1 = 39{,}018.54\,cm^{-1}$, corresponding to principal quantum numbers of the Rydberg electron around 110.

The rotational structure of the spectrum is partially resolved and consists of four rotational branches corresponding to the transitions from rotational levels of the $X^+\,^2\Sigma^+$ state, described by Hund's coupling case (b) and labelled by the quantum number N'' associated with the total angular momentum without spin, to rotational levels of the $A^+\,^2\Pi_{3/2}$ state, described by Hund's coupling case (a) and labelled by the total-angular-momentum quantum number J'. The branches are denoted by the difference $\Delta_{J'N''} = J' - N''$ in Figure 2. The line positions $\tilde{\nu}$ were determined by fitting individual lines with Gaussian

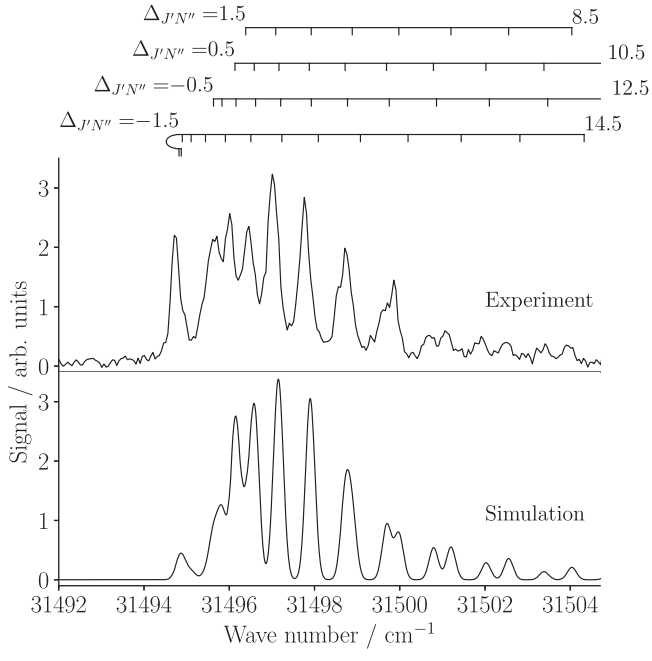

Figure 2. Measured and calculated spectra of the $A^+\,^2\Pi_{3/2}(v' = 1) \leftarrow X^+\,^2\Sigma^+(v'' = 3)$ band of $^{24}MgAr^+$. The assignment bars shown above the spectra give the positions of the transitions to levels of the A^+ state of successive values of J'.

Table 1. Rotational constants of the $X^+\,^2\Sigma^+(v''=3)$ and $A^+\,^2\Pi_{\Omega'}(v'=0,1$ and $5)$ states of $MgAr^+$ determined from the isolated-core multiphoton Rydberg dissociation spectra. The present results for $v'=5$ are compared to the results of [4]. The band origins of the corresponding transitions are also given and compared to available data (see text). The numbers in parentheses correspond to one standard deviation in units of the last digit. All values are in cm^{-1}.

			$B'_{v'}$		$\tilde{\nu}_{v'3}$	
v'	Ω'	B''_3 Present	Present	Literature [4]	Present	Literature [2,4]
			$^{24}MgAr^+$			
0	1/2	0.127(3)	0.195(3)		31,153.7(1)	31,170.7(18)
0	3/2	0.128(4)	0.192(4)		31,230.7(1)	31,246.6(18)
1	1/2	0.125(1)	0.190(1)		31,419.8(1)	31,437.8(18)
	1/2[a]	0.125(1)	0.190(1)		31,419.8(1)	
1	3/2	0.126(2)	0.191(2)		31,496.1(1)	31,515.0(18)
5	1/2	0.127(1)	0.181(1)	0.1836(8)	32,419.3(1)	32,431.6(18)
5	3/2	0.127(1)	0.182(1)	0.1836(8)	32,493.8(1)	32,505.6(18)
			$^{25}MgAr^+$			
1	1/2	0.126(3)	0.188(2)		31,418.7(1)	

[a]Data from a spectrum recorded following excitation to Rydberg states with principal quantum numbers around $n = 78$, instead of around $n = 110$.

functions. The rotational constants B''_3 and $B'_{v'}$ of the initial and final states, respectively, and the origin $\tilde{\nu}_{v'3}$ of the band were then obtained using

$$\tilde{\nu} = \tilde{\nu}_{v'3} + B'_{v'}\left[J'(J'+1) - \Omega'^2\right] - B''_3 N''(N''+1) \quad (1)$$

in a least-squares fit, with $\Omega' = 1/2$ and 3/2 for the $A^+\,^2\Pi_{1/2}$ and $^2\Pi_{3/2}$ spin-orbit components, respectively. The lines below 31,500.5 cm^{-1} consist of several blended rotational lines and were not included in the fit. The fit results are given in Table 1 along with the corresponding 1σ statistical uncertainties of the rotational constants. The statistical uncertainties $\Delta\tilde{\nu}_{v'3}$ of the band origins determined in the least-squares fits are very small. A more conservative estimate of $\Delta\tilde{\nu}_{v'3}$ is given by the standard deviation of the values extracted from several independent spectra of the same vibrational transition, as reported in Table 1. The systematic uncertainty of the band origins is 0.04 cm^{-1} and corresponds to the absolute accuracy of the wave-number calibration. The lower panel of Figure 2 shows the spectrum calculated using the fit results and the rotational line factors for transitions from a state described by Hund's coupling case (b) to a state described by Hund's coupling case (a) [26]. The rotational levels of the initial X^+ state were assumed to be thermally populated at a temperature of 4 K. Overall, the agreement between the measured and calculated spectra is good. However, the intensity of the bandhead of the $\Delta_{J'N''} = -1.5$ branch at lower wave numbers is underestimated by the calculation, and so is the intensity of the first line to its right. These differences may be attributed to the fact that the ions are prepared by photoexcitation from the neutral molecule. Consequently, the real rotational population of the initial state does not follow a pure thermal distribution but is, instead, the result of the interplay between the rotational population of the neutral molecule, the bandwidth of the excitation laser and the rotational line strengths of the transitions involved in the preparation of the ion.

The spectra of $^{25}MgAr^+$ and $^{26}MgAr^+$ can also be measured with the present technique because the different isotopes of Mg ($m = 24$, 25 and 26 u) are resolved in the experimental time-of-flight spectra and can thus be recorded separately. The spectrum of the $A^+\,^2\Pi_{1/2}(v'=1) \leftarrow X^+\,^2\Sigma^+(v''=3)$ transition of $^{25}MgAr^+$ is shown as an example in Figure 3(d). The wave number $\tilde{\nu}_1$ of laser 1 was changed to 39,009.60 cm^{-1} to account for the isotopic shift of the $X^+\,^2\Sigma^+(v''=3) \leftarrow a\,^2\Pi_0$ Rydberg-excitation transition. This wave number corresponds to the excitation of the Rydberg electron to a principal quantum number $n \sim 90$. The lower signal-to-noise ratio results from the lower natural abundance of ^{25}Mg (10%) with respect to ^{24}Mg (79%). The rotational constants of the initial and final states, along with the band origin, can be determined following the method described above, yielding the results given in Table 1. The isotopic shift of the band origin with respect to $^{24}MgAr^+$ is 1.1(2) cm^{-1}. Using this value, we could assign the vibrational band to $v' = 1$ following a standard isotopic-shift analysis (see, e.g. Ref. [2]). This assignment confirms the assignment reported in Ref. [2] for the $A^+\,^2\Pi(v') \leftarrow X^+\,^2\Sigma^+(v''=0)$ transitions when taking into account the energy difference of 284.8(15) cm^{-1} between the $v''=0$ and $v''=3$ vibrational levels of the electronic ground state reported in Ref. [11].

To verify that the Rydberg electron does not influence the core-excitation process, we measured the spectrum of the $A^+\,^2\Pi_{1/2}(v'=1) \leftarrow X^+\,^2\Sigma^+(v''=3)$ transition of $^{24}MgAr^+$ for two different values of the principal quantum number n. The spectra, shown in Figure 3(a,b), were recorded after setting the wave number $\tilde{\nu}_1$ of the Rydberg-excitation laser to 39,018.54 cm^{-1} ($n \sim 110$) and 39,009.60 cm^{-1} ($n \sim 78$), respectively, and are very similar. The band origins and rotational constants

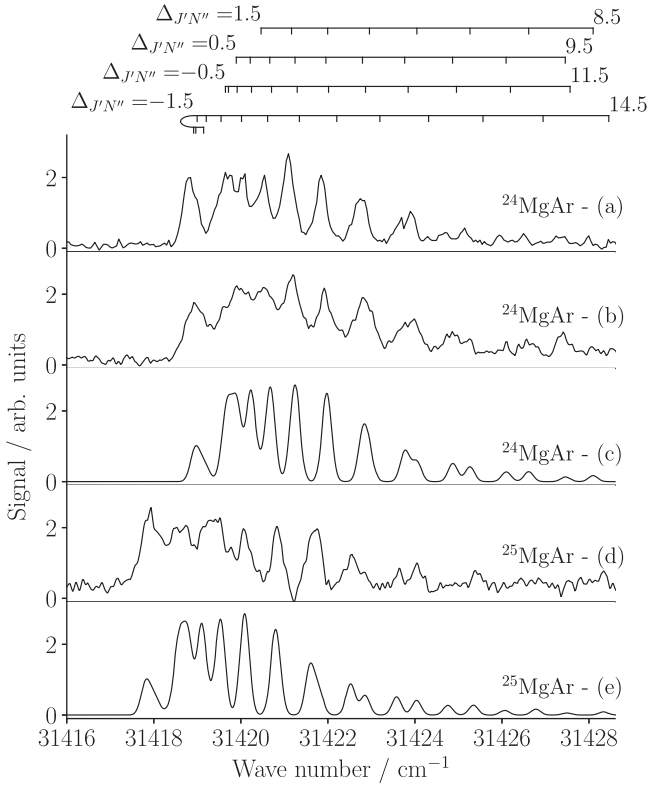

Figure 3. Measured (a, b, d) and calculated (c, e) isolated-core multiphoton Rydberg dissociation spectra of the $A^+\ ^2\Pi_{1/2}(v' = 1) \leftarrow X^+\ ^2\Sigma^+(v'' = 3)$ band of $^{24}MgAr^+$ (a–c) and $^{25}MgAr^+$ (d–e). The spectra (a) and (b) were measured for values of the principal quantum number of the Rydberg electron around 110 and 78, respectively. The assignment bars shown above the spectra give the positions of the transitions to levels of the A^+ state of $^{24}MgAr^+$ of successive values of J'.

derived from their analysis are indistinguishable within the error bars (see Table 1). The widths of individual lines are about 0.2 cm^{-1} in both spectra, which indicates the absence of significant line broadening caused by autoionisation from the A^+ core-excited state. The line widths of autoionizing core-excited Rydberg states are indeed known to scale as $1/n^3$ [27], in which case the line width for $n \sim 80$ should be larger by a factor of 2.6 compared to $n \sim 110$. In the presence of a static electric field with a magnitude large enough to strongly mix the different orbital angular momenta l of the Rydberg electron, a process known as l-mixing, this factor increases to 3.6 because the scaling of the line widths changes to $1/n^4$ [27]. This large change of the line widths with n is clearly not observed in the measured spectra. The widths of the lines in the spectra are, however, larger than the bandwidth of laser 2 (<0.1 cm^{-1}) and are attributed to power broadening, based on the observation that the widths increase when the pulse energy of laser 2 is increased.

The stability of core-excited Rydberg states against autoionisation has been observed and analysed for the Mg atom [20]. When excited in the presence of a static electric field, the dominant decay mechanism of core-excited Rydberg states with principal quantum numbers above $n \sim 75$ is not autoionisation but instead the fluorescence of the excited ionic core, with a rate of 2.6×10^8 s^{-1} for $Mg^+(3p)$ [28]. The line broadening caused by autoionisation is therefore smaller than the natural line width of the isolated-core transition, which is 0.0087 cm^{-1} for the $3s$–$3p$ transition in Mg^+ [28]. The A^+ state of $MgAr^+$ correlates at large internuclear distances with the $3p$ state of Mg^+ and the ground state of Ar. Provided that core-excited Rydberg states of MgAr behave like those of Mg, autoionisation from the A^+ state is expected to be slower than fluorescence and, consequently, should not induce a significant line broadening. This observation is consistent with the present finding that autoionisation from the A^+ state does not affect the recorded spectra. Although no static electric field is applied during the laser excitation in the present experiment, we expect that the stray electric fields generated by the background ions formed by the first laser pulse are sufficient to induce l-mixing and thus to suppress autoionisation until the ion core is dissociated. If the Mg fragments are produced in core-excited Rydberg states, their dominant decay mechanism is also core fluorescence, which explains their detection by PFI after more than 6 μs.

The present values of the band origins are compared to values obtained from data available in the literature [1–4] in Table 1. The latter were calculated, for $v' = 0$ and 1, from the wave numbers of the $A^+\ ^2\Pi(v') \leftarrow X^+\ ^2\Sigma^+(v'' = 0)$ transitions reported by Pilgrim *et al.* [2], using the corrected value of the electronic origin given in Ref. [4] and the $X^+\ ^2\Sigma^+(v'' = 0) - X^+\ ^2\Sigma^+(v'' = 3)$ energy difference of $\Delta_{03} = 284.8(15)$ cm^{-1} from Ref. [11]. The band origins for $v' = 5$ were calculated from the values of the spin-orbit-averaged band origin and spin-orbit splitting reported in Ref. [4] and Δ_{03}. The uncertainties given in the last column of Table 1 are the combined uncertainties of the electronic origin quoted in Ref. [4] and of Δ_{03} from Ref. [11]. The present values of the spin-orbit splittings and relative spacings between the vibrational levels of the A^+ state are in good agreement with the values reported in Refs. [2,4]. However, the values of the absolute transition wave numbers are systematically lower by about 10 to 20 cm^{-1}. We checked for a systematic error in our experiment by calibrating the wave number of laser 2 using two different wave metres. Both results agreed within the specified accuracies. As discussed above, we also verified that the isolated-core transition wave numbers are not affected by

the choice of the range of principal quantum numbers initially excited (see Table 1).

The spin-orbit-averaged value of the electronic origin obtained from the present analysis is 31,477.0(15) cm^{-1} and lies 108 cm^{-1} below the value calculated by Bauschlicher and Partridge [7], and 426 cm^{-1} below the theoretical value of Gaied *et al.* [10]. The present values of the rotational constants for the $v'' = 3$ vibrational level of the electronic ground state of $^{24}MgAr^+$ and $^{25}MgAr^+$ agree within the error bars with the values reported by Wehrli *et al.* [11]. There is also a good agreement between the rotational constants we obtained for the $A^+\ ^2\Pi_{1/2,3/2}(v' = 5)$ states of $^{24}MgAr^+$ and the values reported by Scurlock *et al.* [4].

5. Conclusion

We have presented a new experimental method to study electronic transitions of molecular ions which combines the advantages of REMPD with those resulting from a background-free detection of the fragment ions by PFI of high Rydberg states. The method is closely related to the method of fragment-PIRI spectroscopy [24], from which it differs through the different order in which photodissociation and discrimination of prompt ions are carried out. Our method benefits from the versatility and strength of REMPD for studying electronically-excited states of molecular ions without requiring the use of ion-beam techniques. Moreover, the initial photoexcitation to high Rydberg states allows the preparation of the ionic core in selected (ro)vibrational states. In contrast, ion-beam measurements are typically limited to the quantum states thermally populated in the ion source. In the present study, we exploited this advantage to study the rotational structure of the $A^+\ ^2\Pi(v' = 0)$ state of $MgAr^+$, which can be efficiently excited from the $X^+\ ^2\Sigma^+(v'' = 3)$ state, whereas the Franck-Condon factor governing its excitation from the $X^+\ ^2\Sigma^+(v'' = 0)$ state is very small (see Ref. [2]).

The success of the isolated-core multiphoton Rydberg dissociation technique depends on the facts that (i) Rydberg dissociation is an important decay channel, (ii) the autoionisation rate of the intermediate state is smaller than, or comparable to, the excitation rate to the dissociative state, and (iii) the Rydberg fragment, if in a core-excited state, radiatively decays to a stable state faster than it autoionizes, so that it can still be detected by pulsed-field ionisation several microseconds after photodissociation. These conditions are fulfilled in the case of $MgAr^+$. By applying this method to study the $A^+ - X^+$ band system, we could record spectra with a resolution high enough to resolve the rotational structure and to determine improved values for the band origins.

Acknowledgements

We thank J. A. Agner and H. Schmutz for technical support and C. Kreis for fruitful discussions and experimental help.

Disclosure statement

No potential conflict of interest was reported by the authors.

Funding

This work is supported financially by the Swiss National Science Foundation (Schweizerischer Nationalfonds zur Förderung der Wissenschaftlichen Forschung) (Grant No. 200020-172620) and the European Research Council through an advanced grant under the European Union's Horizon 2020 research and innovation programme (Grant No. 743121).

References

[1] J.S. Pilgrim, C.S. Yeh and M.A. Duncan, Chem. Phys. Lett. **210**, 322–326 (1993).
[2] J.S. Pilgrim, C.S. Yeh, K.R. Berry and M.A. Duncan, J. Chem. Phys. **100**, 7945–7956 (1994).
[3] C.S. Yeh, J.S. Pilgrim, K.F. Willey, D.L. Robbins and M.A. Duncan, Int. Rev. Phys. Chem. **13**, 231–262 (1994).
[4] C.T. Scurlock, J.S. Pilgrim and M.A. Duncan, J. Chem. Phys. **103**, 3293–3298 (1995).
[5] M.A. Duncan, Int. J. Mass Spectrom. **200**, 545–569 (2000).
[6] H. Partridge, C.W. Bauschlicher and S.R. Langhoff, J. Phys. Chem. **96**, 5350–5355 (1992).
[7] C.W. Bauschlicher and H. Partridge, Chem. Phys. Lett. **239**, 241–245 (1995).
[8] D. Bellert and W.H. Breckenridge, Chem. Rev. **102**, 1595–1622 (2002).
[9] A.M. Gardner, C.D. Withers, J.B. Graneek, T.G. Wright, L.A. Viehland and W.H. Breckenridge, J. Phys. Chem. A **114**, 7631–7641 (2010).
[10] W. Gaied, H. Habli, B. Oujia and F.X. Gadea, Eur. Phys. J. D **62**, 371–378 (2011).
[11] D. Wehrli, M. Génévriez, C. Kreis, J.A. Agner and F. Merkt, J. Chem. Phys. A (accepted for publication) (2019).
[12] P.O. Danis, T. Wyttenbach and J.P. Maier, J. Chem. Phys. **88**, 3451–3455 (1988).
[13] Y. Wang, L. Li and W.A. Chupka, Chem. Phys. Lett. **185**, 478–482 (1991).
[14] J.P. Maier, J. Electron Spectrosc. Relat. Phenom. **66**, 15–24 (1993).
[15] S. Willitsch, in *Handbook of High Resolution Spectroscopy*, edited by M. Quack and F. Merkt (John Wiley & Sons, Ltd., Chichester, 2011).
[16] R.S. Freund, in *Rydberg States of Atoms and Molecules*, edited by R. F. Stebbings and F. B. Dunning, (Cambridge University Press, Cambridge, 1983), Chap. 10.
[17] F. Merkt and T.P. Softley, Int. Rev. Phys. Chem. **12**, 205–239 (1993).
[18] W.E. Cooke, T.F. Gallagher, S.A. Edelstein and R.M. Hill, Phys. Rev. Lett. **40**, 178–181 (1978).

[19] P. Camus, T.F. Gallagher, J.M. Lecomte, P. Pillet and L. Pruvost, Phys. Rev. Lett. **62**, 2365–2368 (1989).
[20] D. Wehrli, M. Génévriez and F. Merkt, Phys. Rev. A **100**, 012515 (2019).
[21] M. Génévriez, D. Wehrli and F. Merkt, Phys. Rev. A **100**, 032517 (2019).
[22] H. Krause and H.J. Neusser, J. Chem. Phys. **97**, 5923 (1992).
[23] H. Krause and H.J. Neusser, J. Chem. Phys. **99**, 6278–6286 (1993).
[24] J.G. Goode, J.E. LeClaire and P.M. Johnson, Int. J. Mass Spectrom. Ion Process. **159**, 49–64 (1996).
[25] P.M. Johnson and L. Zhu, Int. J. Mass Spectrom. Ion Process. **131**, 193–209 (1994).
[26] R.N. Zare, *Angular Momentum* (John Wiley & Sons, New York, 1988).
[27] T.F. Gallagher, *Rydberg Atoms* (Cambridge University Press, Cambridge, 1994).
[28] A. Kramida, Yu. Ralchenko, J. Reader and NIST ASD Team, NIST Atomic Spectra Database (ver. 5.7), [Online]. [Wed Oct 16 2019]. National Institute of Standards and Technology, Gaithersburg, MD. 2019. < https://physics.nist.gov/asd > .